The Journal of Chemical Physics

RESEARCH ARTICLE | JANUARY 14 2026

Polymorph selection in charged colloids in the second nucleation step

Special Collection: Self-Assembly: From Blueprints to Breakthroughs

C. Patrick Royall

J. Chem. Phys. 164, 024907 (2026)
https://doi.org/10.1063/5.0305089

The Journal of Chemical Physics ARTICLE pubs.aip.org/aip/jcp

Polymorph selection in charged colloids in the second nucleation step

Cite as: J. Chem. Phys. 164, 024907 (2026); doi: 10.1063/5.0305089
Submitted: 3 October 2025 • Accepted: 22 December 2025 •
Published Online: 14 January 2026

C. Patrick Royall[a)]

AFFILIATIONS

Gulliver UMR CNRS 7083, ESPCI Paris, Université PSL, 75005 Paris, France

Note: This paper is part of the Special Topic, Self-Assembly: From Blueprints to Breakthroughs.
[a)]**Author to whom correspondence should be addressed:** paddy.royall@espci.psl.eu

ABSTRACT

We study polymorph selection in a model of charged colloids, with a focus on the higher-order structure prior to and during nucleation. Specifically, we carry out molecular dynamics simulations of a repulsive Yukawa system with a slightly softened (Weeks–Chandler–Andersen) core. We consider the case where the interaction is long-ranged and the BCC crystal is stable, and also intermediate- and short-ranged cases where the FCC crystal is stable. We use two methods for structure identification, the topological cluster classification (TCC) [A. Malins *et al.*, J. Chem. Phys. **139**, 234506 (2013)] and the bond orientational order parameter analysis of Lechner and Dellago [J. Chem. Phys. **129**, 114707 (2008)]. Under conditions of high supersaturation appropriate to experiments with colloids, we find that the system forms a precursor state in which the particles are hexagonally ordered. That is to say, the precursors are indistinguishable from an HCP crystal using the bond orientational order parameters. This ordering occurs at state points when the body-centered cubic crystal is the stable phase and also when the face-centered cubic crystal is stable. In all cases, the stable polymorph forms from the precursor phase in a second stage. Although at freezing the fluid is much more ordered when the interactions are short-ranged (when FCC is stable), at the supersaturations where nucleation occurs in our simulations, the higher-order structure of the metastable fluids is almost identical for the long-, short-, and intermediate-ranged systems when measured with the TCC.

I. INTRODUCTION

Crystallization is an everyday phenomenon, and although it has been studied for many years, it remains a challenging problem. Crystals may form via homogeneous nucleation, which is a rare event that occurs on a microscopic length scale and timescale.[1] It is hard to access such phenomena in conventional materials, but experiments with colloidal dispersions in which the individual particles can be tracked,[2–6] and computer simulations[7] play an important role in understanding crystal nucleation.

Almost all materials have more than one crystal polymorph with differing thermodynamic stability, depending on the state point. Crucially, the thermodynamic stability may not predict the kinetic stability of the material.[1] This can have spectacular consequences; for example, in the well-known case of the anti-AIDS drug Ritonavir, which formed a previously unknown polymorph, rendering it unusable with very significant patient care consequences, not to mention the cost of $250M.[8–10] Other examples include biomineralization, in which the less stable polymorph of calcium carbonate, aragonite, is formed in a biological setting, yet in the laboratory, the stable form, calcite, is usually found, at least at temperatures appropriate to corals and shells.[11,12]

Understanding of such complex phenomena can be aided by the use of model systems. Here, we consider the Yukawa model with a softened core, which has two polymorphs. This model is well approximated by charged colloids, provided that the degree of electrostatic charge is not too high so that the linear Poisson–Boltzmann approximation in the Derjagiun–Landau–Vervey–Overbeek theory can be used.[13–15] Due to the finite size of the colloidal particles, a hard core is often included, which significantly changes the phase behavior when the Yukawa contribution is weak or short-ranged.[3,14] Often, (when the Yukawa interactions are strong enough and long-ranged enough that the cores do not come into contact), the hard core Yukawa model gives results that are indistinguishable from those in the absence of a core.[16] As shown in the phase diagram in Fig. 1, these polymorphs are FCC in the case that the screening is strong (short range) and BCC when the screening is weak (long range). The triple point (fluid–FCC–BCC coexistence) has also been

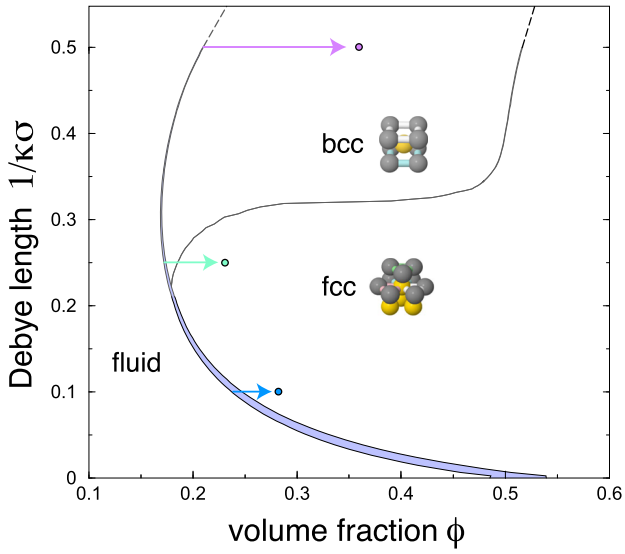

FIG. 1. Phase diagram of the hard core-Yukawa system for a contact potential $\beta\epsilon_{yuk} = 39$. Reproduced with permission from Hynninen and Dijkstra, Phys. Rev. E. **68**, 021407 (2003). Copyright 2003 American Physical Society. The state points shown are the weakest supercooling that crystallized in this study. Arrows indicate the degree of supercooling with respect to the phase boundary. Violet data are the long-ranged case with BCC, the stable polymorph. The blue data are the short-ranged case with BCC, the stable polymorph. Green data are the intermediate-ranged case where, for the supersaturations studied here, FCC is the stable polymorph.

accessed in experiments, where a rather low surface tension between the polymorphs was found.[17]

Now Alexander and McTague[18] argued in general mean-field terms that for simple liquids with a spherically symmetric interaction, BCC is typically to be expected as the first polymorph that forms, and the repulsive Yukawa system forms a suitable testbed for such a prediction. Polymorph selection in Yukawa systems has been studied using computer simulations by Desgranges and Delhommelle,[19] who found that when the interaction was long-ranged, BCC nucleated; yet when the interaction was short-ranged, in addition to the stable FCC phase, BCC was also found, consistent with the ideas of Alexander and McTague.[18] BCC was also found in the FCC-stable regime by Krazter and Arnold[20] and also in some experiments.[21]

In some model systems, precursors, i.e., ordered regions with structure distinct from that of the nucleus, have been found *before* the nucleus forms. In particular, Russo and Tanaka[22] found a hexagonal ordering ahead of FCC nucleation in hard spheres, and Lechner, Dellago, and Bolhuis[23] found hexagonal ordering in the Gaussian core model in the case that the stable phase was both FCC and BCC. In the same model, Russo and Tanaka[24] additionally found a BCC precursor when the stable phase was FCC. In an experimental *tour-de-force*, Tan *et al.*[4] showed evidence for a precursor in experiments on charged colloids, i.e., a hard core Yukawa system. Russo and Tanaka[25] also found a precursor in simulations of water. More recently, using a range of order parameters, de Jager *et al.*[26] found no evidence for precursors in a hard core Yukawa system. Mithen *et al.*[10] performed large-scale simulations of the Gaussian core model, and found (unlike Refs. 23 and 24) that nuclei of mixed BCC, FCC, and HCP composition formed. Clearly, the picture that emerges from this selection of model systems is not entirely consistent. Variations in the state point and perhaps the order parameter used may play a role, a topic to which we return at the end of this study.

Due to their mesoscopic size, colloidal particles exhibit dynamics that are very much slower than in molecular systems.[27] In fact, even without the rare-event sampling methods often used to study molecular systems, it is possible to directly compare nucleation in colloids with brute force (unbiased) computer simulations,[3] and this is the approach we shall employ. Here, we make a detailed study of the structure of nuclei and precursors in a Yukawa system using molecular dynamics simulations. We consider cases where both the BCC and FCC form the stable polymorph, with long-ranged and short-ranged Yukawa interactions, respectively. We also investigate an intermediate case close to the BCC–FCC phase boundary. We use two order parameters to probe the higher-order structure of the nucleating system. First, we investigate the structure of the supersaturated fluid using the topological cluster classification (TCC), which identifies geometric motifs whose bond network is identical to minimum energy clusters of the variable-ranged Morse potential (Fig. 2).[28] Second, we use the bond orientational order (BOOP) parameter method.[29] In particular, we implement the variant introduced by Lechner and Dellago[30] in which second-nearest neighbors are also considered. In the case of both BCC and FCC stable state points, the formation of the nucleus is preceded by a hexagonally ordered structure. This then gives way to the stable polymorph in a second nucleation step.

This study is organized as follows. In the methodology section (Sec. II), we first outline the molecular dynamics simulations used (Sec. II A) before briefly describing the topological cluster classification (Sec. II B) and then the bond orientational order parameter used (Sec. III B). The results are presented in Sec. III. This is broken up into the results from the TCC analysis of the higher-order structure of the bulk fluid prior to nucleation in Sec. III A, followed by the study of the nucleation process using the BOOP (Sec. III B). The structure of the precursors and the surrounding fluid is considered

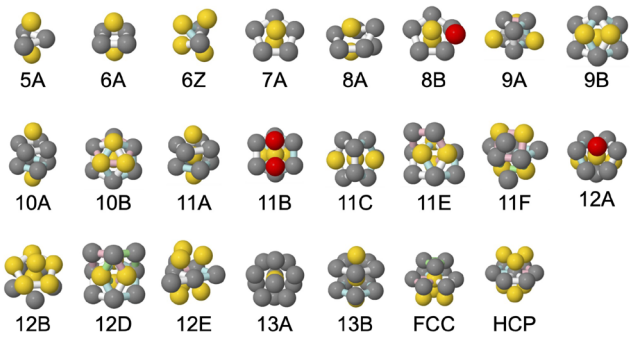

FIG. 2. Higher-order structures identified by the topological cluster classification and crystals. Numbers correspond to the number of particles in the cluster. Letters to the range of the Morse potential ρ_0 for which these are minimum energy clusters [see Eq. (A1) in the Appendix].[31] Reproduced from [Malins *et al.*, J. Chem. Phys. **139**, 234506 (2013)], with the permission of AIP Publishing LLC.

in Sec. III C. Finally, we discuss our findings in Sec. IV and conclude in Sec. V.

II. METHODS

A. Molecular dynamics simulation

As our model, we use a Yukawa system with a slightly softened core, which is representative of charged colloids,[3,32]

$$\beta u_{\mathrm{hyuk}}(r) = \beta u_{\mathrm{wca}}(r) + \beta u_{\mathrm{yuk}}(r), \tag{1}$$

where β is the inverse of the thermal energy $k_B T$.

For the core, we take the Weeks–Chandler–Andersen truncation of the Lennard-Jones interaction,[33]

$$u_{\mathrm{wca}}(r) = \begin{cases} 4\varepsilon_{\mathrm{wca}}\left[\left(\frac{\sigma'}{r}\right)^{12} - \left(\frac{\sigma'}{r}\right)^{6}\right] + \varepsilon_{\mathrm{wca}}, & r \le 2^{\frac{1}{6}}\sigma', \\ 0, & r > 2^{\frac{1}{6}}\sigma', \end{cases} \tag{2}$$

where $\varepsilon_{\mathrm{wca}} = 10 k_B T$ is the interaction energy and r is the separation between two particles of diameter σ'.

The Yukawa potential reads

$$\beta u_{\mathrm{yuk}}(r) = \beta\varepsilon_{\mathrm{yuk}} \frac{\exp\left(-\kappa(r-\sigma')\right)}{r/\sigma'}, \tag{3}$$

where κ is the inverse of the Debye screening length and $\beta\varepsilon_{\mathrm{yuk}}$ is the potential at contact.

To express the potential at contact, we set the unit of length to be the effective hard sphere diameter, defined according to Barker and Henderson,[34]

$$\sigma_{\mathrm{eff}} = \int_0^\infty 1 - \exp\left(-\beta u_{\mathrm{wca}}(r)\right) dr, \tag{4}$$

where $\sigma_{\mathrm{eff}} \approx 1.0786$.

We use σ_{eff} as our unit of length throughout. Henceforth, we drop the subscript x_{eff} and define the interaction parameters as $\kappa\sigma = 2.0, 4.0$, and 10.0 for long, intermediate, and short-ranged cases, respectively. Throughout, we set the contact potential $\beta\varepsilon_{\mathrm{yuk}} = 39.0$. The phase diagram for this model was determined by Hynninen and Dijkstra[16] and is shown in Fig. 1, where $\phi = \pi\rho/(6\sigma^3)$ is the volume fraction and ρ is the number density. Hynninen and Dijkstra[16] consider a perfectly hard core. However, for our parameters, we see no reason to suppose that our system would behave in a significantly different manner.

We use molecular dynamics simulations. While colloids, of course, exhibit overdamped dynamics, in dense fluids, dynamical quantities have been shown to exhibit remarkably little dependence on the particular dynamics used,[35] and indeed, molecular dynamics simulations have been successfully directly compared with experiments on colloids. [36] For the nucleation simulations presented here, we used the NPT ensemble. We set the system size to $N = 11\,664$ or 65 536 for the long-ranged case $\kappa\sigma = 2.0$, $N = 10\,976$ or 87 808 for the intermediate-ranged case $\kappa\sigma = 4.0$, and 16 384 or 87 808 for the short-ranged case $\kappa\sigma = 10.0$. These system sizes are "magic numbers" in the sense that BCC and FCC crystals can form perfect crystals for the long-ranged $(N = 11\,664, 65\,536)$ or intermediate- and short-ranged $(N = 10\,976, 16\,384, 87\,808)$ cases, respectively. We run the system for up to 3×10^6 Lennard-Jones time units, which we take as our unit of time throughout. No qualitative difference was observed between the different system sizes. Renderings are presented for $N = 10\,976, 11\,664, 16\,384$ data.

The simulations were carried out using the LAMMPS package,[37] and we performed at least six runs for each state point. The system was prepared as a set of random coordinates, minimized under Eq. (2) to remove overlaps between particles before the runs were started. We determined the equation of state for the supersaturated fluid, from which we selected the volume fraction at which to launch the nucleation runs.

We find that freezing occurs on the simulation timescale for volume fractions $\phi = 0.356, \ldots, 0.389$ and $0.279, \ldots, 0.300$ for the long-ranged $(\kappa\sigma = 2.0)$, 0.230, ..., 0.284 for the intermediate $(\kappa\sigma = 4.0)$, and $\phi = 0.356, \ldots, 0.389$ for the short-ranged $(\kappa\sigma = 10.0)$ systems, respectively. At higher volume fractions, crystallization occurs rapidly, in a "spinodal-like" manner, as is the case for hard spheres.[6,38]

B. Topological cluster classification

For a complete explanation of the topological cluster classification, Malins *et al.*[28] should be referred to. The topological cluster classification identifies target clusters by their bond network; these are polyhedral, which are associated with a unique bond topology that corresponds to minimum (free) energy clusters of a given interaction potential. The bond network here is defined with a Voronoi decomposition combined with a distance criterion. As the basic building block for clusters, the algorithm constructs all the three-, four-, and five-membered rings that can be constructed along the bond network.

In Fig. 2, we show minimum energy clusters for the Morse potential. Here, the gray particles indicate rings, the yellow particles are spindles, and the red ones are neither spindle nor ring particles. As shown in Eq. (A1) in the Appendix, the Morse potential has a variable range, in that for a given number of particles, the topology of the minimum energy cluster may change for different values of the range parameter ρ_0. Here, we follow the nomenclature of Doye *et al.*,[31] where clusters corresponding to small values of ρ_0 take letters toward the start of the alphabet (e.g., 11A), with progressively larger values of ρ_0 given letters B.., i.e., 11B, 11C, etc. The 6Z cluster is the minimum energy cluster of the Dzugutov potential.[28] For consistency with the BOOP, we set the maximum bond length to the second nearest neighbors, although we note that for these dense systems, the Voronoi construction used will typically dominate in the determination of the bond network.[28] We set the parameter $f_c = 0.82$, which controls the choice between three- and four-membered rings.[28] In our analysis of the bulk liquids (Figs. 3 and 4), we have sampled at least 3×10^6 particles for each state point, and so the statistical errors are relatively small with at least 3×10^3 sampled even for relatively rare clusters.

C. Bond orientational order parameters

We have found the bond orientational order parameter (BOOP) analysis to be a reliable measure of particles in BCC environments[39] and proceed to use the same method here. We also use the BOOP to identify particles in FCC and HCP environments, although very similar results are obtained using the TCC.

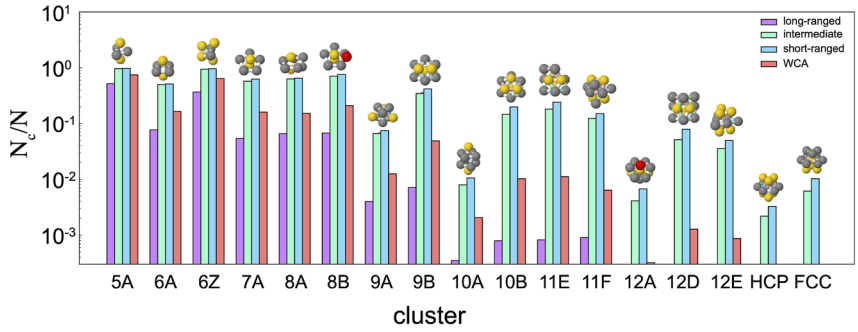

FIG. 3. Population of particles in clusters identified by the topological cluster classification at freezing. Shown are data for the long-ranged system (violet), intermediate (green), short-ranged (blue), and WCA (red). The WCA system is mapped to the freezing point of hard spheres.

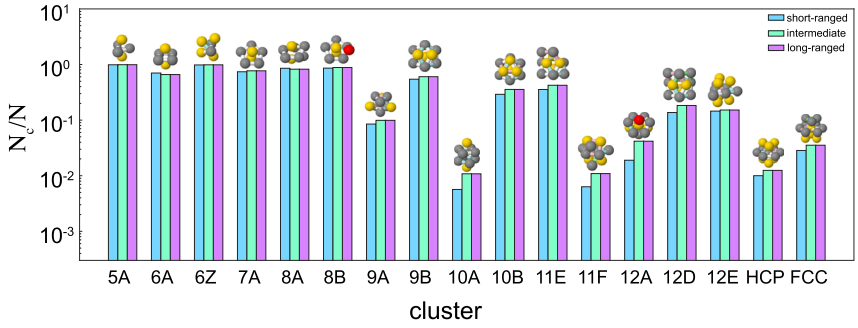

FIG. 4. Population of particles in clusters identified by the topological cluster classification for supersaturated fluids prior to nucleation. Shown are data for the long-ranged system (violet) and short-ranged (blue). The state points shown are $\phi = 0.3597$ and 0.2793 for the long-ranged system and short-ranged system, respectively.

Here, we have followed the method of Lechner and Dellago,[30] who obtained a clear distinction between the crystal structures of interest here by including the second nearest neighbors,

$$Q_{lm} \equiv \frac{1}{n_b} \sum_{\text{bonds}} Y_{lm}(\mathbf{r}), \tag{5}$$

where $Y_{lm}(\mathbf{r})$ are the spherical harmonics with polar and azimuthal angles of the bond between a particle and its neighbors with respect to a fixed reference frame.

The invariant (with respect to the reference frame)

$$Q_l \equiv \sqrt{\frac{4\pi}{2l+1} \sum_{\mathrm{m}=-l}^{l} |Q_{lm}(\mathbf{r})|^2}. \tag{6}$$

The third-order invariants

$$W_l' \equiv \sum_{m_1,m_2,m_3} \begin{Bmatrix} l & l & l \\ m_1 & m_2 & m_3 \end{Bmatrix} Q_{lm_1} Q_{lm_2} Q_{lm_3}, \tag{7}$$

and are normalized as

$$W_l \equiv \frac{W_l'}{\sum_{\mathrm{m}} |\bar{Q}_{lm}(\mathbf{r})|^{3/2}}. \tag{8}$$

Here, in order to include contributions from the second nearest neighbors,[30] we set the bond length to be the second minimum of the radial distribution function $g(r)$ in the (supersaturated) fluid. In the case of crystal phases, we take the fluid at coexistence, or, if the crystal is somewhat more compressed, we take the second minimum of the $g(r)$ at coexistence and scale the range according to $(\phi/\phi_{\mathrm{coex}})^{1/3}$, where ϕ is the volume fraction of interest and ϕ_{coex} is that at coexistence. To evaluate the BOOP, we use the BOP code of Wang *et al.*[40]

III. RESULTS

A. Higher-order fluid structure

We begin our presentation of the results by considering the supercooled liquid prior to crystallization. We compare the higher-order structure (as elucidated with the TCC) at freezing for the long-ranged (BCC stable) and short- and intermediate-ranged (FCC stable) cases in Fig. 3. The data for the long-ranged system [inverse Debye screening length ($\kappa\sigma = 2$) are shown in violet], the intermediate ($\kappa\sigma = 4$) in green, and the short ranged ($\kappa\sigma = 10$) in blue. We see that there is much more higher-order structure for the short-ranged system than the long-ranged case, with the intermediate-ranged case lying in between. For comparison, we also show a Weeks–Chandler–Anderson (WCA) system at freezing (which we take as an effective hard sphere volume fraction $\phi = 0.4917$[6]) for the same value of the WCA interaction strength $\beta\varepsilon_{\mathrm{wca}} = 10$. This, in fact, has somewhat less higher-order structure than the short-ranged system but rather more than the long-ranged case. We note that similar behavior, of a "lack of structure" in a long-ranged system, has been seen previously, albeit for a different interaction potential and under a different mapping.[41]

In our simulations, we find that spontaneous nucleation occurs at rather different degrees of compression with respect to the phase boundary, as shown in Fig. 1. That is $\phi_{\mathrm{nucl}}/\phi_f = 1.73$ for the long-ranged case, while for the short-ranged system it is just $\phi_{\mathrm{nucl}}/\phi_f = 1.18$, and $\phi_{\mathrm{nucl}}/\phi_f = 1.29$ for the intermediate-ranged system, where ϕ_f is the volume fraction of the fluid at freezing.[16] This

corresponds to a pressure scaled by that at freezing of $p/p_f = 3.48$, $p/p_f = 1.63$, and $p/p_f = 1.67$ for the long-, short-, and intermediate-ranged cases, respectively.

Such a large supersaturation of the long-range system before spontaneous nucleation is observed may seem surprising, but it is compatible with the kinetic phase diagram of the Yukawa model.[42] In colloidal systems, the population of TCC clusters typically increases with volume fraction.[3,43] Here, we find the same in Fig. 4, where we show the populations of TCC clusters for simulations at the lowest volume fractions where the system crystallized for the three systems. We sample only the metastable fluid, and to be confident that these are not influenced by nucleation, we take data only for $t < t_{\mathrm{nucl}}/2$, where t_{nucl} is the time at which the nucleus is first detected. Here, the population of TCC clusters is almost indistinguishable in all cases. This shows that the higher-order structure of the fluid before crystallization is almost identical in all three cases.

B. BOOP analysis of polymorph selection

We now turn our attention to the analysis with the bond orientational order parameters (BOOP). We begin by discussing the parameterization of the BOOP, as this exhibited a somewhat unexpected behavior, as shown in Fig. 5. We implement the analysis of Lechner and Dellago (Sec. II C). In particular, we consider the (Q_4, Q_6) and (W_6, Q_6) distributions.

To set parameters to distinguish the structure of interest, we performed NVT simulation of the relevant stable phases. We consider stable crystals of FCC, BCC, and HCP and the fluid at freezing. For the HCP, we used the WCA potential at the (effective) volume fractions of 0.66 and 0.74. For our parameters, we found that this metastable crystal melted when the effective volume fraction was significantly reduced below 0.66. For the crystals, we used a "magic number" of particles to ensure a perfect crystal, 10 976, 8192, and 8000 for FCC, BCC, and HCP, respectively. We used 10 976 particles for the fluid, and we considered two state points corresponding to the long ranged and short ranged cases. For the BCC and FCC, we considered the melting volume fraction and also a somewhat higher volume fraction (around 25% higher). A complete list of state points sampled is provided in Table I in the Appendix.

TABLE I. State points used to parameterize the BOOP in Fig. 5. The lower volume fraction for BCC and FCC was taken at melting.

State	ϕ	$\kappa\sigma$
Fluid	0.2368	10.0
Fluid	0.208	2.0
Fluid	0.492	WCA
FCC_m	0.2468	10.0
FCC	0.35	10.0
HCP	0.661	WCA
HCP	0.741	WCA
BCC	0.21	2.0
BCC	0.315	2.0

In the scatter plots shown in Figs. 5(a) and 5(b), we see a clear distinction between the different crystal phases in both plots and indeed the fluid. For the fluid at freezing, we saw no difference between the long-ranged, short-ranged, or WCA systems and do not distinguish the points in Fig. 5. Likewise, the BCC and melting at higher volume fraction showed no difference and are not distinguished. However, in the case of the FCC at melting, although we saw no sign of melting in the simulations, the (Q_4, Q_6) scatter plot in Fig. 5(a) shows that this state point is quite different from that at higher volume fraction. Indeed, the distribution of data points overlaps with BCC. This overlap disappears in the (W_6, Q_6) scatter plots, and we use this to distinguish the polymorphs, as shown by the gray lines in Fig. 5(b). No meaningful difference in the results was found in the case that we used the (Q_4, Q_6) distributions to distinguish the crystal structures. The Q_6 distributions of the FCC at melting and the HCP are shown in Fig. 5(c), showing that with our cutoff criterion of $Q_6 = 0.107$, there is some small overlap for the tail of each distribution. It is interesting to inquire as to the origins of the difference in the BOOP distributions in the FCC at melting and at higher volume fraction. While we leave a full investigation for the future, we did probe the structure with the TCC. In the case of the denser crystal, all particles were identified as FCC. In the case of the FCC at

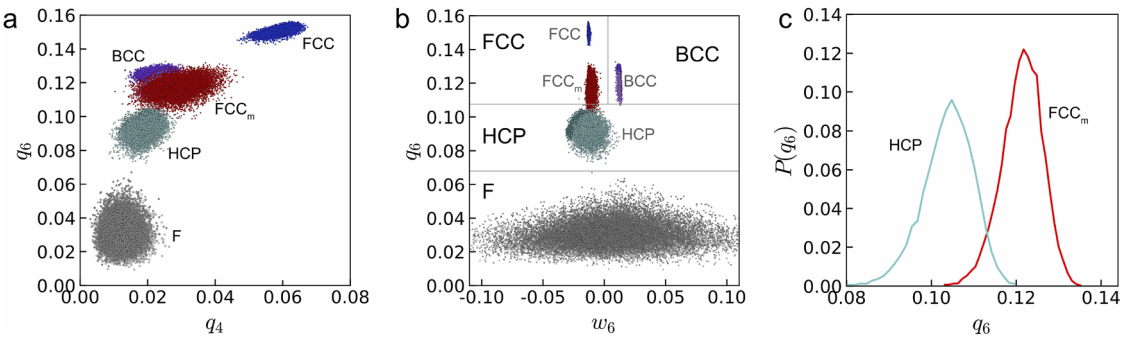

FIG. 5. Bond orientational order parameters for polymorphs considered. (a) q_4–q_6 representation. (b) w_6–q_6 representation. In (a) and (b), the data are colored as fluid (gray), BCC (violet), HCP (teal), and FCC (blue). FCC at melting (FCC_m) is shown in red. Lines in (b) indicate regions identified with the structures indicated in black type. The gray type refers to data from simulations for each state point. (c) Probability distribution of q_6 for the HCP (teal) and FCC at melting (red) states. Here, the teal line is HCP and the red is FCC at melting. Further details of the state point samples are provided in Table I in the Appendix.

melting, 99.66% of particles were identified as FCC, so we conclude that these criteria of Q_6, W_6 are reasonable for our purposes.

We now analyze the process of nucleation using the BOOP. In Fig. 6, we show the population of particles classified as supercooled liquid (gray), BCC (violet), HCP (teal), and FCC (blue). The results

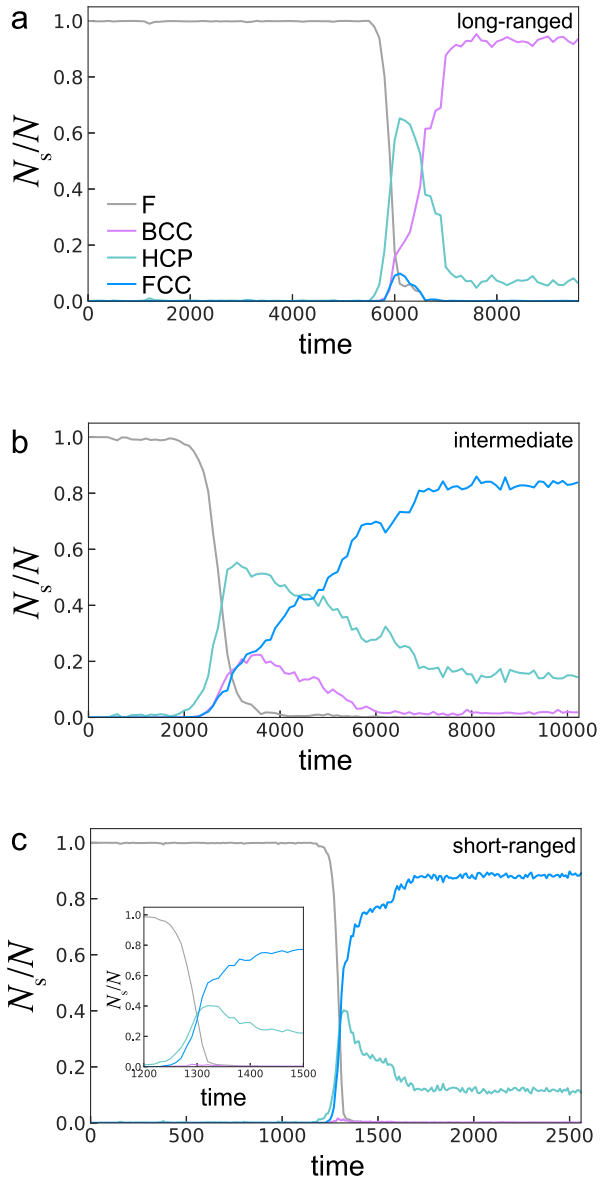

FIG. 6. Time dependence of the population of particles in different environments as characterized by the bond orientational order parameter. (a) Long-ranged case. Here, the initial volume fraction is $\phi = 0.363$ and the pressure is $p = 93.66 k_B T/\sigma^3$. (b) Intermediate-ranged case. Here, the initial volume fraction is $\phi = 0.363$ and the pressure is $p = 15.93 k_B T/\sigma^3$. (c) Short-ranged case. Here, the initial volume fraction is $\phi = 0.279$ and the pressure is $p = 8.368 k_B T/\sigma^3$. The inset shows the same data zoomed in around the nucleation time. Time is expressed in Lennard-Jones time units, and the colors correspond to fluid (gray), BCC (violet), HCP (teal), and FCC (blue).

for the long-, intermediate-, and short-ranged systems are shown in Figs. 6(a)–6(c), respectively. In all cases, we see an increase in the HCP population just prior to the nucleation event when the system transforms to BCC (long ranged) or FCC (short- and intermediate-ranged). In the case of the intermediate-ranged system, we see a significant quantity of BCC before this population falls as the FCC population continues to rise and the nuclei grow. We note that this state point lies close to the BCC-stable region in the phase diagram (Fig. 1). Similar behavior is seen for other state points, as shown in Fig. 12 in the Appendix.

We therefore interpret these HCP regions as precursor nuclei to the stable phase, which forms a little later. This is qualitatively similar to the results of Lechner, Dellago, and Bolhuis[23] and Russo and Tanaka,[24] who also found HCP precursors to nucleation in the Gaussian core model for these same polymorphs.

A sequence of snapshots for the short-ranged system is shown in Fig. 7. Here, we see that the HCP (teal) forms first, then initially small regions of mainly FCC (blue) with some BCC (violet) form within the nucleus. At slightly longer times, more FCC particles are seen in the center of the nucleus. As the nucleus grows, the center becomes more dominated by FCC, surrounded by an HCP layer with a trace quantity of BCC at the FCC–HCP interface.

In Fig. 8, we show a snapshot of a precursor nucleus for the long-ranged (a) and intermediate (b) systems. The long-ranged case is for $t = 5700$, and the time-evolution for this run is shown in Fig. 6(a). We see that at this time, there is very little BCC, and that the ordering (interpreted with the BOOP) is HCP, i.e., precursors. In the intermediate-ranged case (b), the snapshot is taken at $t = 2330$, by which time considerable amounts of BCC and FCC have formed [see Fig. 6(b)], and indeed both can be seen in the middle of the ordered region. The coexistence of both polymorphs is broadly consistent with the experimental observation of a low surface tension between the two.[17]

C. TCC analysis of precursor nuclei

What is the nature of these precursors identified as HCP? In Fig. 9, we see in the time-evolution of the TCC cluster populations that the populations of the 6A octahedron, 11F, and 12E all increase just as the precursor forms. This occurs in both the longer-ranged [Fig. 9(a)], intermediate (b), and short-ranged (c) systems. In the long-ranged case [Fig. 9(a)], more than half the system is identified in the HCP precursor state, and the populations of 6A, 8A, 11F, and 12E all remain high. In the short-ranged run shown, the populations of these clusters were rather less at long times (presumably they are less compatible with the FCC here).

None of these clusters are strictly compatible with the HCP structure. We infer that the precursors, while they are hexagonally ordered (Fig. 8), may not be perfect HCP crystals. It is also worth noting that the TCC identification can tolerate some degree of distortion in the bond network. Inspection of the bond orientational order parameter analysis (Fig. 5) shows that the HCP is found between the BCC (or FCC at melting) and the fluid for both the (Q_4, Q_6) and (W_6, Q_6) representations. Therefore, while the precursor undoubtedly shows considerable ordering, it may be distinct from being a full crystal phase.

We further probe the structure of the HCP precursors as follows. In Fig. 10, we show the distribution in the number of selected

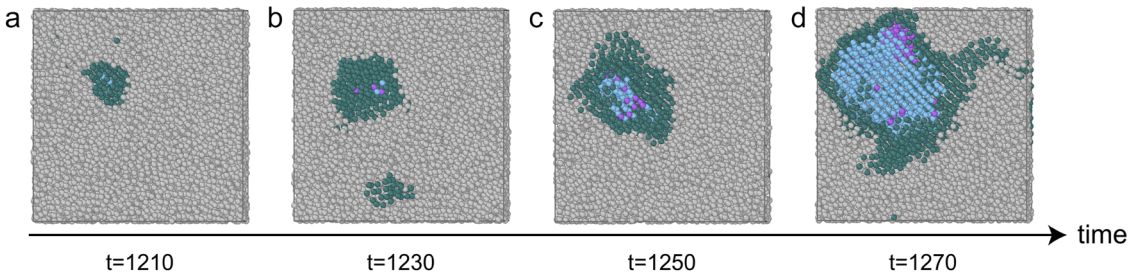

FIG. 7. Snapshots at selected times during a nucleation run showing (a) the initial nucleus identified as HCP, (b) the growing nucleus with small amounts of FCC, and (c) the emergence of BCC and FCC domains as the nucleus continues to grow. At (slightly) longer times, an FCC domain decorated by HCP precursor particles is seen. Here, particles identified as fluid are shown in gray, HCP in teal, and FCC in blue. We consider the short-ranged system at an initial volume fraction of $\phi = 0.279$.

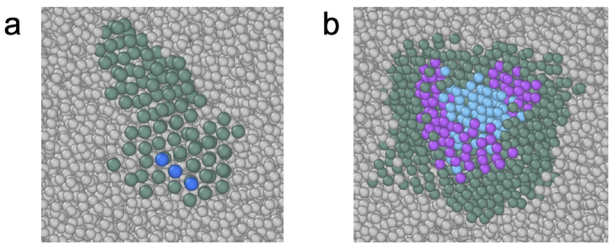

FIG. 8. Precursor particles with hexagonal order. Particles identified as fluid are shown in gray, HCP in teal, FCC in blue, and BCC in violet. (a) Long-ranged system at an initial volume fraction of $\phi = 0.363$. This snapshot is taken at $t = 5700$ prior to the formation of the BCC. (b) Intermediate-ranged system at an initial volume fraction of $\phi = 0.230$. This snapshot is taken at $t = 2300$.

clusters a precursor particle is found in. (For the HCP cluster itself, particles are found in 1 or 2 HCP clusters.) We see a number of particles in up to 18 6A octahedra. Although the 6A is not strictly compatible with the HCP, as noted earlier, some distortion can be tolerated in the bond network. For larger clusters, the 8A has, in fact, some compatibility with the HCP crystal (though less than for the FCC[44]), and the 11F has a degree of HCP-like character.[28] We note that the 5A triangular bipyramid is compatible with the HCP crystal. In Fig. 13(a) in the Appendix, we show the same analysis for the intermediate-ranged system, which shows a very similar distribution. The same holds for the short-ranged system (data not shown). We further show in Fig. 13(b) the same analysis for a bulk HCP crystal. The distributions of the number of particles in the clusters are broadly similar, although there are some quantitative differences. However, at the level of this analysis, it is hard to be sure whether these are true differences between the precursors and the bulk HCP or whether this relates to the fact that many of the precursor particles are at interfaces with the fluid, which, of course, is not the case for the bulk HCP (with periodic boundary conditions). This suggests that there is no significant difference in the structure of the precursors insofar as we can discern here. While further work is needed, we conclude that the precursors identified as HCP are consistent with an HCP crystal.

We now consider the effect of these precursor nuclei on the surrounding fluid. It has previously been shown that FCC nuclei

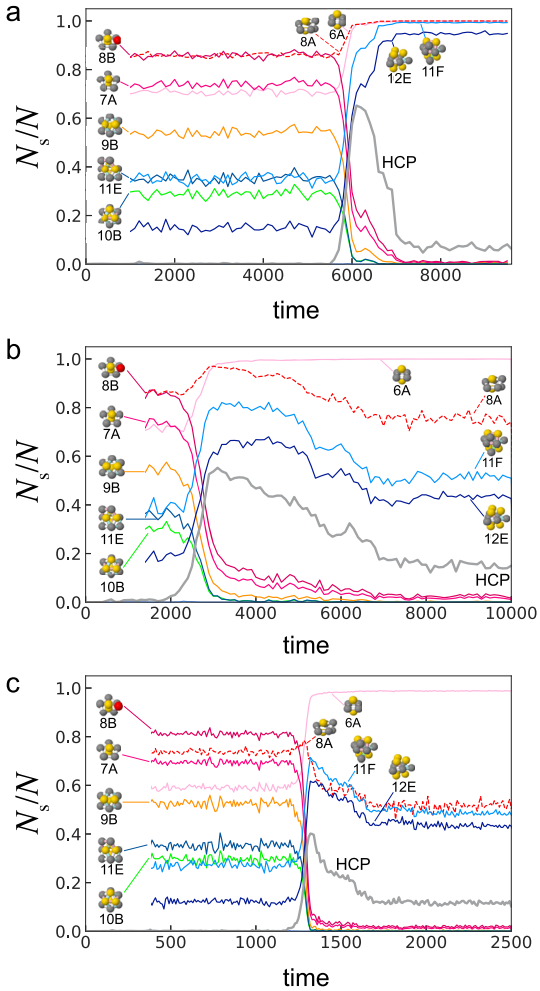

FIG. 9. Time dependence of the population of particles in TCC clusters; also shown is the population of HCP precursors identified with the BOOP. (a) Long-ranged case. Here, the initial volume fraction is $\phi = 0.363$ and the pressure is $p = 93.66 k_B T/\sigma^3$. (b) Intermediate-ranged case. Here, the initial volume fraction is $\phi = 0.230$ and the pressure is $p = 15.94 k_B T/\sigma^3$. (c) Short-ranged case. Here, the initial volume fraction is $\phi = 0.279$ and the pressure is $p = 8.368 k_B T/\sigma^3$.

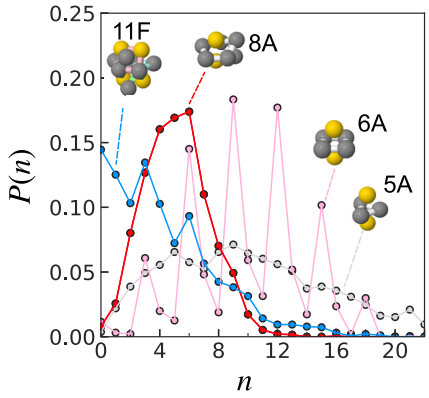

FIG. 10. TCC analysis of particles in HCP precursors. Shown is the distribution of the number of TCC clusters in which *n*, a precursor particle, is found. Here, we show data for the long-ranged system.

tend to suppress local fivefold symmetric order in the liquid for hard spheres.[44] Indeed, the formation of FCC may be controlled by adjusting the degree of fivefold symmetry in the liquid.[45] We perform the same analysis as that carried out by Gispen *et al.*[44] to show the effect of the hexagonally ordered precursor nucleus on the liquid. Here, then, we find that, like the case for hard spheres, there is significant suppression of fivefold symmetry in the liquid due to the hexagonally ordered nucleus [Fig. 11(b)]. That is, the population of 7A pentagonal bipyramids is suppressed close to the nucleus, as indicated by the darker violet.

It was also shown that there was an enhancement of the dodecahedral 8A cluster on the edge of FCC nuclei, which was argued to promote the selection of that polymorph. Here, for these HCP-like precursors, instead we see an enhancement of 6A octahedra relative to the fluid [Figs. 11(a), 11(c), and 11(d)]. (The same rendering for the 8A dodecahedron is shown in Fig. 14 in the Appendix.)

IV. DISCUSSION

Like Russo and Tanaka[22] with hard spheres and the Gaussian Core Model,[24] and Lecher and Dellago with the GCM,[23] we find a hexagonally ordered precursor to the formation of the BCC and FCC nuclei in the Yukawa system with a slightly softened core. Our results are also compatible with the experimental study of Tan *et al.*[4] They are not in alignment with a study that found no precursors in the hardcore Yukawa system,[26] although that study used a somewhat different approach. It seems that a systematic study of different model systems with a range of order parameters would be desirable in the near future. Nevertheless, some comments regarding the apparent discrepancy between this study and that of de Jager *et al.*[26] are in order. That work considered somewhat different parameters, namely a fully hard core and a contact potential of $\beta\varepsilon_{\text{yuk}} = 81.0$. Perhaps more significantly, a different implementation of the BOOP was employed, namely the so-called solid angle nearest neighbor method, rather than the next-nearest neighbors considered here. While a proper investigation would be needed to be sure, it is possible that the precursors identified here as HCP were identified as the stable crystal in that study.

The regime of supersaturation that we have explored is relatively small (Sec. II A). A key challenge then is to determine over what domain of supersaturation such precursors are found. Considering the results of Mithen *et al.*[10] for the GCM, it is possible that the hexagonally ordered precursors might not be found at weaker supercooling.

In the future, it would be attractive to perform simulations at weaker supersaturations than have been possible here, using, for example, forward flux sampling or umbrella sampling. This would enable one to probe to what extent these hexagonally ordered precursors are found as the degree of supersaturation falls. Given the drop in higher-order structure in the BCC-stable long-ranged case, notably the disappearance of hexagonally ordered HCP and FCC (Fig. 3, violet data), it is tempting to imagine that the proposal by Alexander and McTague of BCC ordering in general[18] may be expected, consistent with the findings of Refs. 19 and 20.

We have found that the TCC cluster populations, as a measure of the higher-order structure, are very similar for all three systems for state points where nucleation was found on the simulation timescale. The TCC clusters are themselves minimum energy clusters of the variable-ranged Morse potential, Eq. (A1), Fig. 2. Now, of course, the interactions here are not Morse interactions, and indeed they are even repulsive. Yet it is possible, in the spirit of the WCA treatment of the Lennard-Jones interactions, i.e., to truncate and shift at the minimum of the potential, to do the same with the Morse interaction [Eq. (A2) in the Appendix]. It turns out that such truncated Morse interactions have a very similar higher-order structure

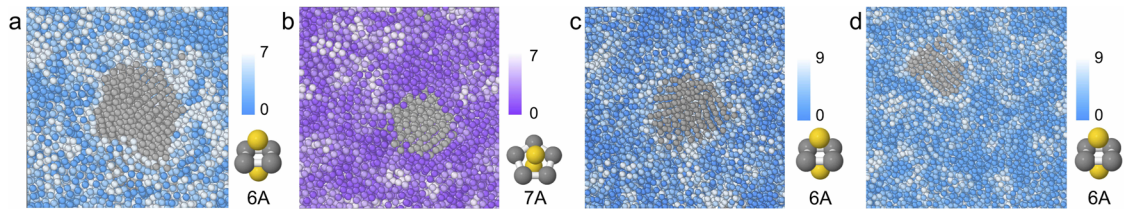

FIG. 11. Higher-order fluid structure around the hexagonally ordered precursors. Here, we show how many of a specific cluster a particle is in. For example, in (a), a white particle is in 7 6A octahedra. (a) Short-ranged system, $\phi = 0.279$ at $t = 1100$. The gray particles are precursors. The blue shading denotes the number of 6A octahedra a particle is in. (b) Long-ranged system, $\phi = 0.363$ at $t = 5700$. The gray particles are precursors. The violet shading denotes the number of 7A pentagonal bipyramids a particle is in. (c) Long-ranged system, $\phi = 0.363$ at $t = 5700$. The gray particles are precursors. The blue shading denotes the number of 6A octahedra a particle is in. (d) Intermediate-ranged system, $\phi = 0.230$ at $t = 2100$. The gray particles are precursors. The blue shading denotes the number of 6A octahedra a particle is in.

to the full potential, as indeed the WCA has to the full Lennard-Jones potential.[41]

Such a "truncated Morse" interaction may then be compared with the Yukawa interaction used. We find values of the Morse range parameter $\rho_0 \approx 2.5$ for the longer-ranged, $\kappa\sigma = 2.0$ case and $\rho_0 \approx 4.0$ for $\kappa\sigma = 10.0$. For reference, the Lennard-Jones interaction corresponds to a still shorter interaction of $\rho_0 \approx 6.0$.[31] Now it turns out that the minimum energy structures for $\rho_0 = 2.5$ and $\rho_0 = 4.0$ are identical except for $m = 11$ and $m = 12$. Therefore, even applying this line of reasoning to the populations of TCC clusters, we would in fact expect them to be similar here, despite the change in the interaction range. This is what we find. Therefore, it seems reasonable that polymorph selection here occurs in the hexagonal precursor state. Determining why this hexagonally ordered state can form both polymorphs stands as an interesting question for the future.

It is interesting to consider the transformation of the HCP precursors into BCC and FCC. Similar solid–solid transformations have been considered previously.[46] The extent to which these are thermally activated would be an interesting question. In principle, it is not expected that HCP forms in the first place. In this soft matter system, we speculate that its transformation to the stable polymorph is thermally driven, and it would be an intriguing question to probe in detail in the future.

V. CONCLUSION AND OUTLOOK

We have studied nucleation in a model polymorphic system using molecular dynamics simulations. We find a hexagonally ordered precursor to both the BCC and FCC crystals, each of which forms (after the precursor) when it is the stable phase. The BCC is stable for a long-ranged interaction (here the inverse screening length $\kappa\sigma = 2.0$), while the FCC is stable for an intermediate ($\kappa\sigma = 4.0$) and short-ranged interaction ($\kappa\sigma = 10.0$), Fig. 1. The precursors suppress the fivefold symmetry of the surrounding fluid in a similar manner to FCC nuclei in hard spheres.[44]

In our simulations, which examine spontaneous nucleation (on timescales relevant to experiments with colloids[3,4]), a much higher supersaturation is needed to observe nucleation for long-ranged interactions than is the case for shorter-range interactions. This is consistent with our observation of a fluid with much less order at freezing in the case of a long-ranged interaction when compared to a shorter-ranged case.

In the future, it would be attractive to carry out this kind of analysis on state points with weaker supersaturation than are accessible to our direct simulations. Determining any difference between the precursors in the case that FCC is nucleated and BCC is nucleated stands as an interesting challenge. While the precursors in both satisfy our criteria for HCP (Fig. 6), it is tempting to imagine that there is some subtle difference in their structure that somehow encodes that one forms FCC and the other BCC. However, our analysis found no such difference. In addition, other systems, for example, colloids with attractive interactions, could be investigated with the same methodology. It would also be interesting to extend this approach to other classes of materials. (Non-hexagonally ordered) precursors have been found in water[25] and NiAl[47] and may be relevant in more complex systems such as calcium carbonate solution, a model system for biomineralization.[48]

ACKNOWLEDGMENTS

It is a pleasure to acknowledge Marjolein Dijkstra for many inspiring conversations around nucleation, hardcore Yukawa systems, and polymorph selection, and Bob Evans, Daan Frenkel, Yi-Yeoun Kim, Fiona Meldrum, David Quigley, John Russo, Richard Sear, Frank Smallenburg, and Hajime Tanaka for many conversations on the topic of nucleation and polymorph selection. CPR acknowledges the Agence Nationale de Recherche for the grant DiViNew.

AUTHOR DECLARATIONS

Conflict of Interest

The author has no conflicts to disclose.

Author Contributions

C. Patrick Royall: Conceptualization (equal); Data curation (equal); Formal analysis (equal); Funding acquisition (equal);

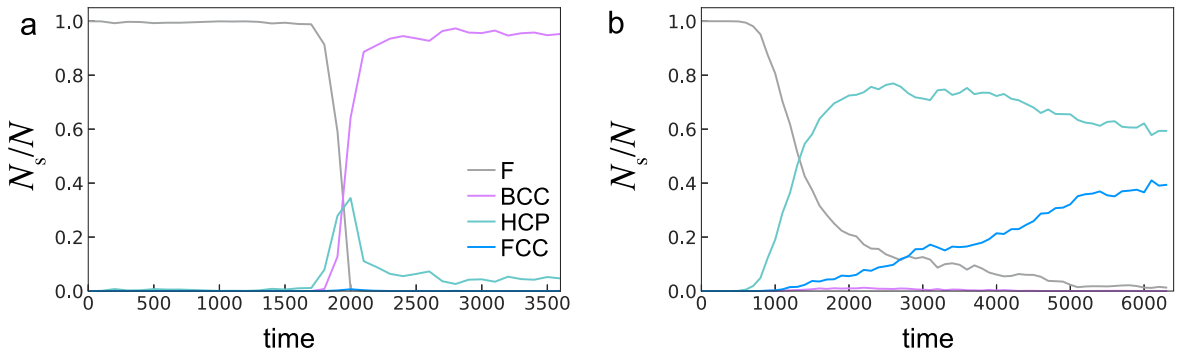

FIG. 12. Time dependence of the population of particles in different environments as characterized by the bond orientational order parameter. (a) Long-ranged case. Here, the initial volume fraction is $\phi = 0.377$ and the pressure is $p = 95.64 k_B T/\sigma^3$. (b) Short-ranged case. Here, the initial volume fraction is $\phi = 0.2813$ and the pressure is $p = 9.564 k_B T/\sigma^3$. Time is expressed in Lennard-Jones time units, and the colors correspond to fluid (gray), BCC (violet), HCP (teal), and FCC (blue).

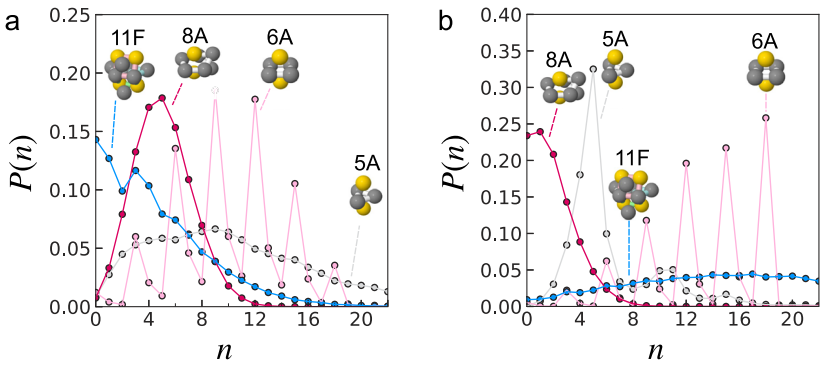

FIG. 13. TCC analysis of particles in HCP precursors and bulk HCP crystal. Shown is the distribution of the number of TCC clusters in which n, a precursor particle, is found. Here, we show data for the intermediate-ranged system (a) for $\phi = 0.230$ and a bulk HCP crystal (b) where $\phi = 0.661$.

Investigation (equal); Methodology (equal); Project administration (equal); Resources (equal); Software (equal); Validation (equal); Visualization (equal); Writing – original draft (equal); Writing – review & editing (equal).

DATA AVAILABILITY

The data that support the findings of this study are available from the corresponding author upon reasonable request.

APPENDIX: SUPPLEMENTARY DATA AND MODEL DETAILS

The topological cluster classification identifies minimum energy clusters. Here, we consider minimum energy clusters from the Morse potential, which reads

$$\beta u_{\text{morse}}(r) = \beta\varepsilon_{\text{morse}}\left[e^{-2\rho_0(r-\sigma)} - 2e^{-\rho_0(r-\sigma)}\right], \tag{A1}$$

where ρ_0 controls the range of the interaction and, therefore, the topology of the clusters in Fig. 2 as determined by Doye, Wales, and Berry.[31]

It is possible, in the spirit of the WCA treatment of the Lennard-Jones interaction, to define a truncated and shifted Morse potential that retains only the repulsive part,

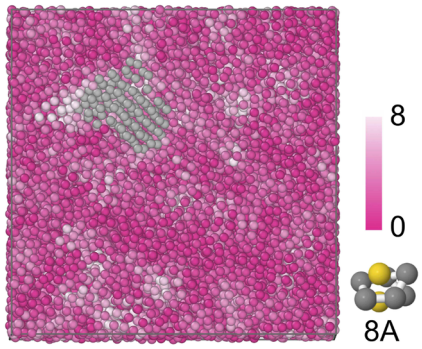

FIG. 14. Rendering showing how many 8A dodecahedra a particle is in. Short ranged system, $\phi = 0.279$. The gray particles are precursors. The pink shading denotes the number of 8A dodecahedron a particle is in.

$$u_{\text{tm}}(r) = \begin{cases} \beta\varepsilon_{\text{morse}}\left[e^{-2\rho_0(r-\sigma)} - 2e^{-\rho_0(r-\sigma)} + 1\right], & r \le \sigma, \\ 0, & r > \sigma. \end{cases} \tag{A2}$$

One can compare $u_{\text{tm}}(r)$ to the Yukawa potential with the softened core Eq. (1) and select a value of ρ_0 that best matches Eq. (1). We arrive at $\rho_0 \approx 2.5$ for the long-ranged case $\kappa\sigma = 2.0$ and $\rho_0 \approx 4.0$ for the long-ranged case $\kappa\sigma = 10.0$. For the full Morse potential, $\rho_0 \approx 6.0$ is rather close to the Lennard-Jones interaction.

REFERENCES

[1] R. P. Sear, "The non-classical nucleation of crystals: Microscopic mechanisms and applications to molecular crystals, ice and calcium carbonate," Int. Mater. Rev. **57**, 328–356 (2012).
[2] U. Gasser, E. R. Weeks, A. Schofield, P. N. Pusey, and D. A. Weitz, "Real-space imaging of nucleation and growth in colloidal crystallization published by: American association for the advancement of science linked references are available on JSTOR for this article: Real-space imaging of nucleation and growth in," Science **292**, 258–262 (2001).
[3] J. Taffs, S. R. Williams, H. Tanaka, and C. P. Royall, "Structure and kinetics in the freezing of nearly hard spheres," Soft Matter **9**, 297 (2013).
[4] P. Tan, N. Xu, and L. Xu, "Visualizing kinetic pathways of homogeneous nucleation in colloidal crystallization," Nat. Phys. **10**, 73–79 (2014).
[5] A. Ivlev, H. Löwen, G. E. Morfill, and C. P. Royall, *Complex Plasmas and Colloidal Dispersions: Particle-Resolved Studies of Classical Liquids and Solids* (World Scientific Publishing Co., Singapore, 2012).
[6] C. P. Royall, P. Charbonneau, M. Dijkstra, J. Russo, F. Smallenburg, T. Speck, and C. Valeriani, "Colloidal hard spheres: Triumphs, challenges, and mysteries," Rev. Mod. Phys. **96**, 045003 (2024).
[7] G. C. Sosso, J. Chen, S. J. Cox, M. Fitzner, P. Pedevilla, A. Zen, and A. Michaelides, "Crystal nucleation in liquids: Open questions and future challenges in molecular dynamics simulations," Chem. Rev. **116**, 7078–7116 (2016).
[8] D.-K. Bučar, R. W. Lancaster, and J. Bernstein, "Disappearing polymorphs revisited," Angew. Chem., Int. Ed. **54**, 6972–6993 (2015).
[9] J. Bauer, S. Spanton, R. Henry, J. Quick, W. Dziki, W. Porter, and J. Morris, "Ritonavir: An extraordinary example of conformational polymorphism," Pharm. Res. **18**, 859–866 (2001).
[10] J. P. Mithen, A. J. Callison, and R. P. Sear, "Nucleation of crystals that are mixed composites of all three polymorphs in the Gaussian core model," J. Chem. Phys. **142**, 224505 (2015).
[11] F. C. Meldrum and H. Cölfen, "Controlling mineral morphologies and structures in biological and synthetic systems," Chem. Rev. **108**, 4332–4432 (2008).

[12]M. Zeng, Y.-Y. Kim, C. Anduix-Canto, C. Frontera, D. Laundy, N. Kapur, H. K. Christenson, and F. C. Meldrum, "Confinement generates single-crystal aragonite rods at room temperature," Proc. Natl. Acad. Sci. U. S. A. **115**, 7670–7675 (2018).
[13]C. P. Royall, M. E. Leunissen, and A. v. Blaaderen, "A new colloidal model system to study long-range interactions quantitatively in real space," J. Phys.: Condens. Matter **15**, S3581–S3596 (2003).
[14]C. P. Royall, M. E. Leunissen, A.-P. Hyninnen, M. Dijkstra, and A. van Blaaderen, "Re-entrant melting and freezing in a model system of charged colloids," J. Chem. Phys. **124**, 244706 (2006).
[15]I. Rios de Anda, A. Statt, F. Turci, and C. P. Royall, "Low-density crystals in charged colloids: Comparison with Yukawa theory," Contrib. Plasma Phys. **55**, 172–179 (2015).
[16]A. P. Hynninen and M. Dijkstra, "Phase diagrams of hard-core repulsive Yukawa particles," Phys. Rev. E **68**, 021407 (2003).
[17]M. Chaudhuri, E. Allahyarov, H. Löwen, S. Egelhaaf, and D. A. Weitz, "Triple junction at the triple point resolved on the individual particle level," Phys. Rev. Lett. **119**, 128001 (2017).
[18]S. Alexander and J. McTague, "Should all crystals be bcc? Landau thoery of solification and crystal nucleation," Phys. Rev. Lett. **41**, 702–705 (1978).
[19]C. Desgranges and J. Delhommelle, "Polymorph selection during the crystallization of yukawa systems," J. Chem. Phys. **126**, 054501 (2007).
[20]K. Kratzer and A. Arnold, "Two-stage crystallization of charged colloids under low supersaturation conditions," Soft Matter **11**, 2174–2182 (2015).
[21]S. Xu, H. Zhou, Z. Sun, and J. Xie, "Formation of an fcc phase through a bcc metastable state in crystallization of charged colloidal particles," Phys. Rev. E **82**, 010401 (2010).
[22]J. Russo and H. Tanaka, "The microscopic pathway to crystallization in supercooled liquids," Sci. Rep. **2**, 505 (2012).
[23]W. Lechner, C. Dellago, and P. G. Bolhuis, "Role of the prestructured surface cloud in crystal nucleation," Phys. Rev. Lett. **106**, 085701 (2011).
[24]J. Russo and H. Tanaka, "Selection mechanism of polymorphs in the crystal nucleation of the Gaussian core model," Soft Matter **8**, 4206–4215 (2012).
[25]J. Russo and H. Tanaka, "Crystal nucleation as the ordering of multiple order parameters," J. Chem. Phys. **145**, 211801 (2016).
[26]M. de Jager, F. Smallenburg, and L. Filion, "In search of a precursor for crystal nucleation of hard and charged colloids," J. Chem. Phys. **159**, 134902 (2023).
[27]W. Russel, D. Saville, and W. Schowalter, *Colloidal Dispersions* (Cambridge University Press, Cambridge, 1989).
[28]A. Malins, S. R. Williams, J. Eggers, and C. P. Royall, "Identification of structure in condensed matter with the topological cluster classification," J. Chem. Phys. **139**, 234506 (2013).
[29]P. J. Steinhardt, D. R. Nelson, and M. Ronchetti, "Bond-orientational order in liquids and glasses," Phys. Rev. B **28**, 784–805 (1983).
[30]W. Lechner and C. Dellago, "Accurate determination of crystal structures based on averaged local bond order parameters," J. Chem. Phys. **129**, 114707 (2008).
[31]J. P. K. Doye, D. J. Wales, and R. S. Berry, "The effect of the range of the potential on the structures of clusters," J. Chem. Phys. **103**, 4234–4249 (1995).
[32]C. P. Royall, W. C. K. Poon, and E. R. Weeks, "In search of colloidal hard spheres," Soft Matter **9**, 17–27 (2013).
[33]J. D. Weeks, D. Chandler, and H. C. Andersen, "Role of repulsive forces in determining the equilibrium structure of simple liquids," J. Chem. Phys. **54**, 5237 (1971).
[34]J. A. Barker and D. Henderson, "What is 'liquid'? Understanding the states of matter," Rev. Mod. Phys. **48**, 587–671 (1976).
[35]L. Berthier and W. Kob, "The Monte Carlo dynamics of a binary Lennard-Jones glass-forming mixture," J. Phys.: Condens. Matter **19**, 205130 (2007).
[36]C. P. Royall, A. A. Louis, and H. Tanaka, "Measuring colloidal interactions with confocal microscopy," J. Chem. Phys. **127**, 044507 (2007).
[37]S. Plimpton, "Fast parallel algorithms for short-range molecular dynamics," J. Comput. Phys. **117**, 1–19 (1995).
[38]E. Zaccarelli, C. Valeriani, E. Sanz, W. C. K. Poon, M. E. Cates, and P. N. Pusey, "Crystallization of hard-sphere glasses," Phys. Rev. Lett. **103**, 135704 (2009).
[39]T. S. Ingebrigtsen, J. C. Dyre, T. B. Schroder, and C. P. Royall, "Crystallisation instability in glassforming mixtures," Phys. Rev. X **9**, 031016 (2019).
[40]Y. Wang, S. Teitel, and C. Dellago, "Melting of icosahedral gold nanoclusters from molecular dynamics simulations," J. Chem. Phys. **122**, 214722 (2005).
[41]J. Taffs, A. Malins, S. R. Williams, and C. P. Royall, "The effect of attractions on the local structure of liquids and colloidal fluids," J. Chem. Phys. **133**, 244901 (2010).
[42]W. Gispen and M. Dijkstra, "Kinetic phase diagram for nucleation and growth of competing crystal polymorphs in charged colloids," Phys. Rev. Lett. **129**, 098002 (2022).
[43]C. P. Royall, S. R. Williams, and H. Tanaka, "Vitrification and gelation in sticky spheres," J. Chem. Phys. **148**, 044501 (2018).
[44]W. Gispen, G. M. Coli, R. van Damme, C. P. Royall, and M. Dijkstra, "Crystal polymorph selection mechanism of hard spheres hidden in the fluid," ACS Nano **17**, 8807–8814 (2023).
[45]J. Taffs and C. P. Royall, "The role of fivefold symmetry in suppressing crystallization," Nat. Commun. **7**, 13225 (2016).
[46]M. Li, Z. Yue, Y. Chen, H. Tong, H. Tanaka, and P. Tan, "Revealing thermally-activated nucleation pathways of diffusionless solid-to-solid transition," Nat. Commun. **12**, 4042 (2021).
[47]Y. C. Hu and H. Tanaka, "Revealing the role of liquid preordering in crystallisation of supercooled liquids," Nat. Commun. **13**, 4519 (2022).
[48]R. Demichelis, P. Raiteri, J. D. Gale, D. Quigley, and D. Gebauer, "Stable prenucleation mineral clusters are liquid-like ionic polymers," Nat. Commun. **2**, 590 (2011).